IEEE Access
Multidisciplinary | Rapid Review | Open Access Journal

SPECIAL SECTION ON GIGAPIXEL PANORAMIC VIDEO WITH VIRTUAL REALITY

Received July 24, 2020, accepted August 16, 2020, date of publication August 21, 2020, date of current version September 2, 2020.

Digital Object Identifier 10.1109/ACCESS.2020.3018453

Optimization and Simulation of Garden Image Visual Effect Based on Particle Swarm and Wavelet Threshold

HUA ZHANG[1] AND XIONGFEI MIN[2]
[1]School of Fine Arts, Weinan Normal University, Weinan 714099, China
[2]School of Physical Education, Weinan Normal University, Weinan 714099, China
Corresponding author: Xiongfei Min (minxiongfei@wnu.edu.cn)

ABSTRACT This paper optimizes and simulates the visual effects of garden graphics based on particle swarm and wavelet threshold algorithm, and uses deep belief networks as the main body of the classifier. To make up for the shortcomings of the activation function of the deep belief network, this paper adopts the wavelet basis function as the activation function of the deep belief network to improve the recognition accuracy of the deep belief network, especially the recognition accuracy of small changes in the garden image information. It analyzes the learning process of deep belief network in detail, finds out the shortcomings of traditional algorithms, and optimizes them, combined with particle swarm optimization algorithm to construct a wavelet deep belief network model to further improve the recognition accuracy and recognition speed of garden image recognition. A hybrid optimization algorithm of genetic and particle swarm algorithms is proposed. The two algorithms complement each other and the idea of crossover and variation is introduced into the standard Particle Swarm Optimization (PSO) algorithm to avoid premature convergence of solutions obtained by the PSO algorithm and lead to local optimal solutions. Seven optimal solutions obtained by the algorithm are used as the weight of the sample features, which are multiplied by the sample features to obtain the input data of the weighted K-nearest neighbor algorithm. After that, a three-fold cross-validation method is utilized to train the data to ensure the classification effect of the data set. The weighted K-nearest neighbor algorithm has the best classification effect based on the hybrid optimization of genetic algorithms and particle swarm algorithm.

INDEX TERMS Particle swarm, wavelet threshold, garden image, visual effect, optimized simulation.

I. INTRODUCTION

As the carrier of information transmission, voice, image, and video occupy a dominant position. Images are ubiquitous in people's lives and work [1]. Compared with the use of hearing to gather information, the use of vision to obtain information can be more comprehensive. Depending on the research, the use of vision to obtain information in human senses accounts for more than 70% [2]. It is precisely because the image as a visual carrier is so important, with the advancement of human science and technology, digital image processing technology came into being. Nowadays, digital image processing technology has been extensively used in many fields such as mathematics, economy, industry, agriculture, medicine and so on. However, in the process of digital image acquisition, transmission and conversion, due to the mechanical movement of the equipment, the internal circuit of the system, the equipment and materials themselves, the image will be stained with different degrees of noise, which will seriously reduce the image quality [3]. If a good noise reduction effect is not achieved in the image preprocessing stage, it will further cause some trouble in the subsequent deep processing of the image, so the noise reduction processing of the image is very important [4]. While reducing noise, the target edge of the image will also become blurred due to filtering, which is extremely detrimental to the image quality. Therefore, how to protect the edge of the image target while decreasing noise is a topic worthy of study [5]. Today, in the field of landscape architecture, most of the landscape architecture has been closely linked to computer science, supporting, and relying on each other, and most of the landscape architecture has become the service target of computer technology [6]. With

The associate editor coordinating the review of this manuscript and approving it for publication was Zhihan Lv.

the infiltration of computer science into the discipline of landscape architecture, its impact on the discipline of landscape architecture is long-lasting and can be overlooked [7]. Combined with computer science, the design method of landscape architecture has the characteristics of high efficiency, speed, and accuracy, and its colors are rich and easy to modify [8]. Brings a whole new era to the discipline of landscape architecture. In everyday life, photos of natural gardens are the most common and used image data [9]. This kind of image on the Internet is also increasing. In addition to the functions of providing appreciation and adjustment, the subject of landscape gardening a large amount of this kind of data is also needed for planning, design, and classification of landscape elements [10]. Correctly classifying landscape elements in geological scenery images to improve the speed of reading and searching by designers has become a problem that we need to solve. So far, basic image classification technology is limited to the underlying visual features of the image [11].

Since the 1970s, digital image technology has gradually begun to have its technical characteristics, and has a relatively complete system, and has gradually become a relatively independent subject [12]. Until the mid-1970s, image understanding began to develop slowly, and computer vision theory gradually entered people's field of vision [13]. Shao J *et al.* developed the gray-level co-occurrence matrix, and they also studied the relationship with human visual perception [14]. Six texture features: roughness, directionality, regularity, similarity, contrast, and roughness have become the basis for studying image texture features [15]. Among swarm intelligence algorithms, the PSO algorithm was proposed by Kandhway P *et al.* in 1995 and has attracted a lot of attention from researchers [16]. The PSO algorithm has the advantages of fast convergence speed, high-quality solutions, and high robustness in terms of optimization, but at the same time, with each continuous iteration of the population, the similarity between particles is getting higher and higher [17]. The shortcomings of particles easily falling into the local optimum and not easily jumping out of the local optimum are particularly obvious. Researchers improve the PSO algorithm in terms of parameter settings, population disturbance, and assignment, and combination with other algorithms to improve the performance of the algorithm [18]. Maulucci G first introduced an inertial weight, which used the inertial weight to ensure the influence of the velocity of particles in flight, thereby enhancing the search and exploration capabilities of particles in the population [19]. Since then, countless researchers have conducted related research based on the improved PSO algorithm. The article also proposes a strategy to dynamically adjust the value of the inertia weight, so that the value of the inertia weight shows a linear decrease trend with the iteration [20]. When the algorithm is in the initial stage, the particles in the population have strong search capabilities. When iterating to the later stage, the smaller inertia weight can ensure the optimization near the optimal position; Majumdar A *et al.* proposed a time-varying the PSO algorithm of the acceleration factor has been extended twice to improve the performance of the algorithm [20]; Zhang Y *et al.* applied the Gaussian mutation operator to the PSO algorithm to maintain the diverse distribution of the population [21]. The results show that it is better than the pure PSO algorithm, etc.; also, for the PSO algorithm in the multi-objective optimization problem, Ebbini ES *et al.* proposed an optimization algorithm based on chaotic mutation, which optimizes the understanding of the size distribution [22]. And Shahmiri L *et al.* proposed a strategy idea of a competition mechanism, which makes the particles change the learning strategy in the iterative process, using the competition and cooperation mechanism to replace the original learning method, and the improved learning method can effectively improve the diversity of particles in the population [23]; Heo YJ *et al.* proposed the idea of using the strong local exploration ability of the differential evolution algorithm to make up for the shortcomings of the PSO algorithm, so that the PSO algorithm and the differential algorithm can be used in different periods [24]. In the application research of PSO algorithm, Wang Y *et al.* realized recursive network design by using two evolutionary learning algorithms of genetic algorithm and PSO algorithm [25]; Reily B *et al.* once proposed a two-stage PSO algorithm to solve the random shop scheduling problem [26]; Chandrasekar KS once proposed a multi-objective feature selection method based on PSO algorithm and fusion of cross operation, mutation operation and crowded distance technology, and named CMDPSO, through this method can obtain a better feature subset set, etc.; as more scholars join in the more in-depth research on the PSO algorithm, the PSO algorithm will be used in more fields the PSO algorithm has been applied to practical problems, and the research on practical problems will become more and more perfect and mature [27].

Aiming at the limitations of the traditional wavelet hard and soft threshold functions proposed by Donoho, and referring to the research results of previous literature, the traditional wavelet threshold function is improved. The improved wavelet threshold function can effectively avoid the Pseudo-Gibbs phenomenon caused by the wavelet hard threshold function, and solve the problem of low image reconstruction accuracy owing to the constant deviation between the estimated wavelet coefficient and the original wavelet coefficient. Through simulation and comparative experiments, we can know that the improved wavelet threshold function can improve the effect of image noise reduction. Because the target edge and noise in the image belong to high-frequency information, in the filtering process, the image target edge will also become blurred. Bilateral filtering can alleviate this problem, but the limitation of traditional bilateral filtering is that irrelevant pixels in the filtering window will also participate in the filtering, which is not conducive to filtering the central pixel. Therefore, a gray-scale filter kernel function is improved to reduce the influence of irrelevant pixels in the filter window to the center pixel to be filtered and to improve the ability of bilateral filtering to protect the edge of the image target. To ensure that the research

results are more reliable, after the simulation and comparison experiment, the image quality evaluation indicators include the Mean-Square Error (MSE) and Peak Signal to Noise Ratio (PSNR), Structural Similarity (SSIM) is also introduced. SSIM is an index for judging the degree of similarity between the gray value and detail characteristics of the image after the noise reduction process and the original image, which can make the data result more convincing. After verifying the feasibility of the algorithm, combining the improved wavelet threshold function and the improved bilateral filtering, a comparative experiment is designed to reduce the noise of the somber image with Gaussian noise. In-depth analysis and evaluation of the results of simulation experiments reflect the practical application value of the improved combined algorithm set out in the present paper.

II. PARTICLE SWARM WAVELET THRESHOLD GRAPHIC OPTIMIZATION DESIGN

A. ANALYSIS OF IMPROVING PARTICLE SWARM COMBINED WITH A WAVELET THRESHOLD ALGORITHM

Particle Swarm Optimization is an algorithm proposed by Dr. Eberhart and Dr. Kennedy. Fundamentally speaking, it is a technological method of evolutionary calculation [28]. The predation behavior of birds the proposal of this algorithm has inspired. The basic idea of the PSO optimization algorithm is to use the collaboration and information sharing between different individuals in the biological group to find the ''optimal solution'' in this information. The advantage of this algorithm is it is very simple, easy to implement, and without too many parameter adjustments. In my mind, imagine this picture: there is a set of seagulls searching for fish in a sea area. There is only a school of fish in this sea area, but all the seagulls in the sky do not know the specific location of the fish in the sea. However, these seagulls know the distance between their position and the fish [29]. Then, the most simple and effective method in the optimal strategy for finding the fish is to search the current distance to the fish. The sea area around the nearest seagull. At this time, seagulls are abstracted as particles or points without mass and volume and can extend to n-dimensional space. The position of particle m in M-dimensional space is generally expressed by formula (1):

$$M_i = (m_1, m_2, \ldots, m_N) \tag{1}$$

Formula (2) can express the flight speed:

$$U_i = (\mathrm{u}_1, \mathrm{u}_2, \ldots, \mathrm{u}_N) \tag{2}$$

The fitness value (FV) of each particle is determined by the objective function, and at the same time, they know their current position U and the best position best they can find. This can be seen as the particle's private flight experience. Also, each particle can know the best position best (the optimal value is best) that can be searched by all particles in the entire group so far. This can be viewed as the experience of the particle companion. Through the particles' own flight experience and the experience of their companions, the particles can determine the next movement trajectory and movement direction [30]. The PSO algorithm obtains a group of randomly moving particles through the step of random initialization. After that, the continuous iterative search to get an optimal solution. In the process of ''iteration'', each particle must update itself. This step needs to be carried out by tracking two ''extreme'' (poet, best). After finding these two optimal values in the steps, the particles update their speed and position through formulas (3) and (4):

$$U_i = (\mathrm{u}_1, \mathrm{u}_2, \ldots, \mathrm{u}_N) \tag{3}$$

$$U_i = \mathrm{u}_i + c_1 \times rand() + c_2 \times rand() \tag{4}$$

This article introduces the non-negative inertia weight factor W into the formula. U means that the particle always maintains the inertia of motion, so that it tends to expand the search space, while still having the ability to continue to explore additional unknown areas. The formulas are shown in (5) and (6):

$$Y_i = y_i + c_1 \times rand() + c_2 \times rand() \tag{5}$$

$$K_i = Y_i + N_i \tag{6}$$

The framework of the improved particle swarm optimization algorithm is presented in figure 1.

Wavelet can perform the local transformation in the time domain and frequency domain and can observe the signal gradually from coarse to fine, and then extract operational information from the signal, which solves many difficult problems that the Fourier transform cannot solve [31]. The wavelet transform is defined as:

$$K_i(a, b) = \int_{-\infty}^{+\infty} f(t)\phi_{a,b}(t)dt \tag{7}$$

The inverse transformation is:

$$f(a, b) = \frac{1}{C_\varphi}\int_{-\infty}^{+\infty} f(t)\phi_{a,b}(t)dt \tag{8}$$

$$C_\varphi = \int_{-\infty}^{+\infty} \frac{\left|\phi_{a,b}(t)\right|^2}{w}dw \tag{9}$$

The wavelet can be obtained by scaling and shifting the basic wavelet. The basic wavelet is a real-valued function with fast attenuation and satisfies the integration of zero in the domain of definition, namely:

$$\int_{-\infty}^{+\infty} \frac{\left|\phi_{a,b}(t)\right|^2}{w}dw = 0 \tag{10}$$

Its spectrum satisfies:

$$B_\varphi = \int_{-\infty}^{+\infty} \frac{\left|\phi_{a,b}(t)\right|^2}{w}dw \tag{11}$$

Therefore, the basic wavelet has sound attenuation in the frequency domain. A set of wavelet basis functions can be generated from basic wavelets through scale and displacement factor:

$$\phi_{a,b}(t) = \frac{1}{\sqrt{a}}\int_{-\infty}^{+\infty} \frac{\left|\phi_{a,b}(t)\right|^2}{w}dw \tag{12}$$

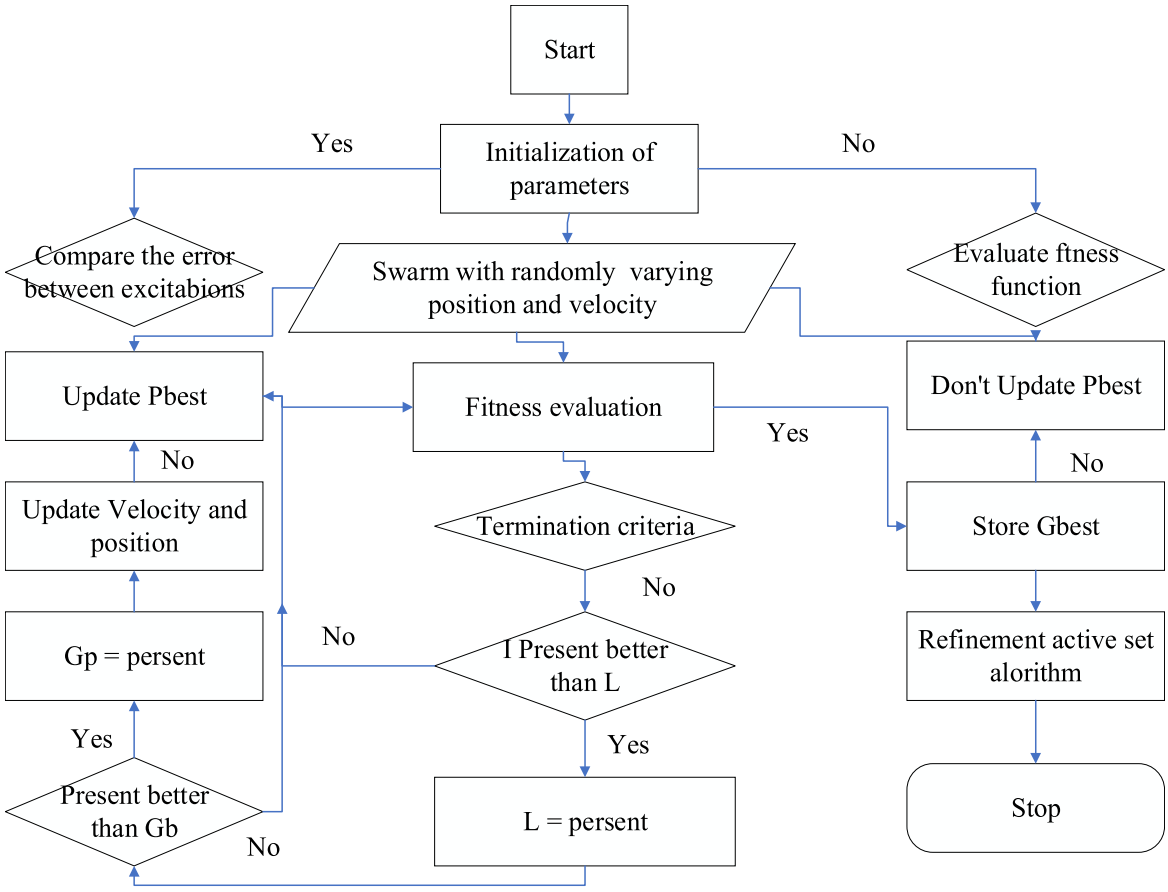

FIGURE 1. Improved example full optimization algorithm.

Using the wavelet threshold function method to denoise an image or signal requires three necessary processes. First, use the selected wavelet base to perform wavelet multi-level decomposition of the signal to be de-noised, the decomposition level is determined according to needs, and then the decomposed wavelet coefficients are obtained; secondly, the selected wavelet threshold function is used to decompose the wavelet coefficients. Finally, the threshold quantized wavelet coefficients are reconstructed according to the inverse process of the decomposition mechanism to obtain the restored signal. The restored signal is the result of noise reduction processing.

A digital image will be decomposed into four components after the first wavelet decomposition, including a low-frequency component A1 and three high-frequency components. The three high-frequency components can be subdivided into horizontal high-frequency components H1 and vertical directional high-frequency component V1 and diagonal high-frequency component D1. Among them, the low-frequency component is mainly the area where the gray-level changes in the digital image are relatively smooth, including the main content depicted in the image; while the high-frequency component is mainly the area where the gray-level changes more drastically in the digital image or the gray value is more abrupt area, such as the edge of the target in the image and the noise in the image. The second-level wavelet decomposition is to decompose the low-frequency component A1 from the first-level decomposition according to the above rules. It can continue to decompose to obtain a low-frequency component A2, the horizontal high-frequency component H2, the vertical high-frequency component V2, and the diagonal high-frequency component D2. By analogy, wavelet multi-level decomposition can be realized. In the actual noise reduction process, different decomposition scales can be selected according to different requirements to adapt to digital images with distinct characteristics. The higher the decomposition scale, the larger the corresponding calculation amount, and the longer the system response time. However, it is not necessary that the higher the decomposition scale, the better the noise reduction effect, and it is necessary to choose the best choice. Figure 2 shows in the schematic diagram of the wavelet two-level decomposition [32].

For a noisy digital image, after noise reduction processing, the quality of the processed image is evaluated to judge the quality of the noise reduction algorithm. Image quality evaluation is mainly divided into subjective evaluation and objective evaluation. Subjective evaluation is based on anthropological eyes, visually and related experience to evaluate image quality. The advantage of this method is

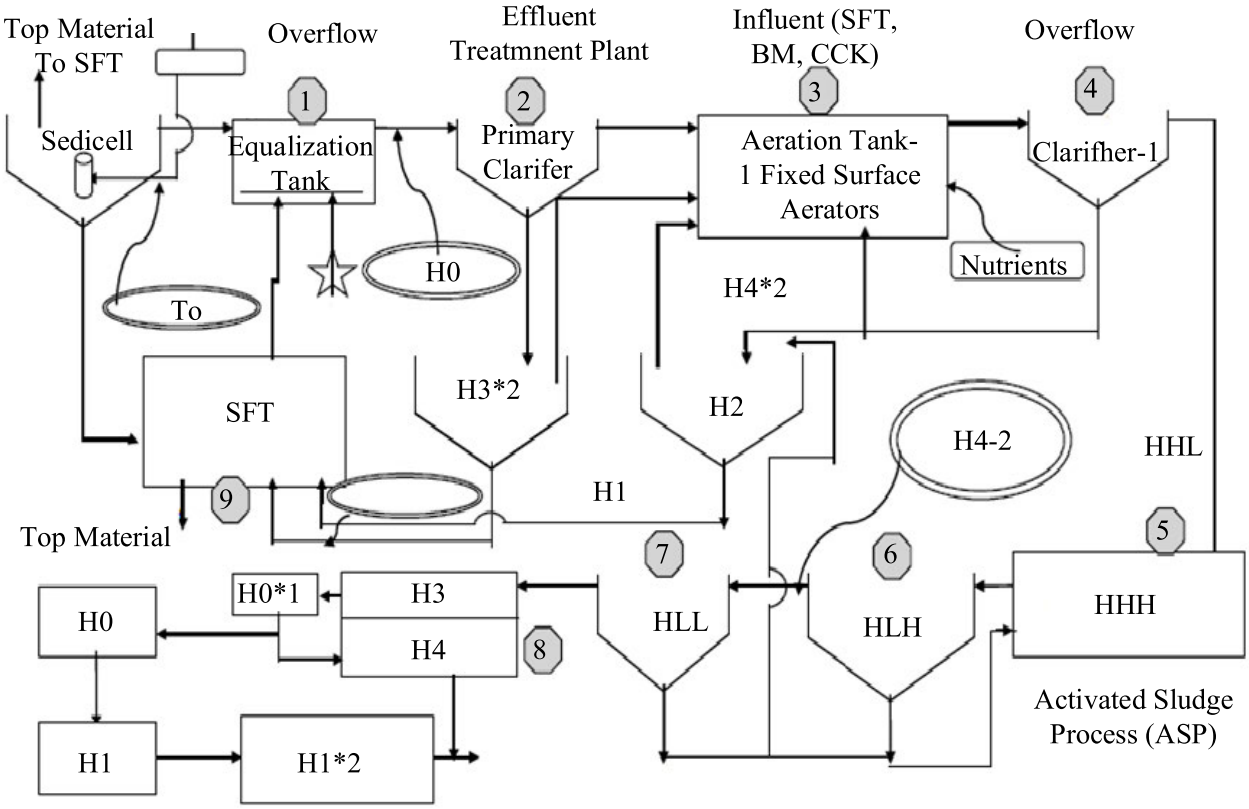

FIGURE 2. Schematic diagram of wavelet two-level decomposition.

simple and fast, and greatly improves the time efficiency; its disadvantage is that it can only perform a qualitative evaluation of images, but cannot achieve a quantitative evaluation. Moreover, there are certain subjective factors, different evaluation criteria, and low reference values for the evaluation results. Therefore, a fair assessment of the image quality is particularly important. The data results provide an accurate understanding of the quality of the digital image and the advantages and disadvantages of the noise reduction algorithm, which requires further analysis and processing. This paper uses three objective image quality evaluation mechanisms, namely Mean-Square Error (MSE), Peak Signal to Noise Ratio (PSNR) and Structural Similarity (SSIM). The three evaluation mechanisms all have reference image quality evaluation, that is, the original clear image without noise is needed to participate in the calculation [33].

The expression of mean square error MSE is:

$$MSE = \frac{1}{MN} \cdot \sum_{j=1}^{N} \sum_{i=1}^{M} [F(i,j) - f(i,j)]^2 \tag{13}$$

The expression of the peak signal-to-noise ratio PSNR is:

$$PSNR = 1.5 \times 1g(255^2/MSE) \tag{14}$$

The expression of structural similarity SSIM is:

$$\text{SSIM(F, f)} = \frac{(y_i + c_1 \times rand)(\text{C})}{(\text{C}_1)(y_i + c_1 \times rand())} \tag{15}$$

B. GRAPHIC OPTIMIZATION MODEL DESIGNS

The current network model establishment mainly includes four parts: the determination of the number of network layers, the selection of initial weight, the determination of the number of neurons, and the selection of activation functions. According to empirical analysis, when network model has more layers, its training accuracy will be higher, but as the number of network layers continues to increase, the complexity of its neural network will also increase, increasing in its training time, convergence speed is relatively slow, increasing the load of the computer, the requirements on the computer are also higher. According to empirical analysis, when network model has more layers, its training accuracy will be higher. However, as the number of network layers continues to increase, the complexity of its neural network will also increase, increasing in its training time, convergence speed is relatively slow, increasing the load of the computer, the requirements on the computer are also higher. The selection of the initial weight of network model has a very significant influence on the establishment of the network model.

If the initial weight is set to be large, it is easy to saturate the output layer excitation function during training, resulting in the loss function gradient value is very small or even zero, resulting in the training network is interrupted and the next step of learning cannot be carried out [34]. This strategy can guarantee that the network output value is in the maximum range of the change of the excitation function, and meets

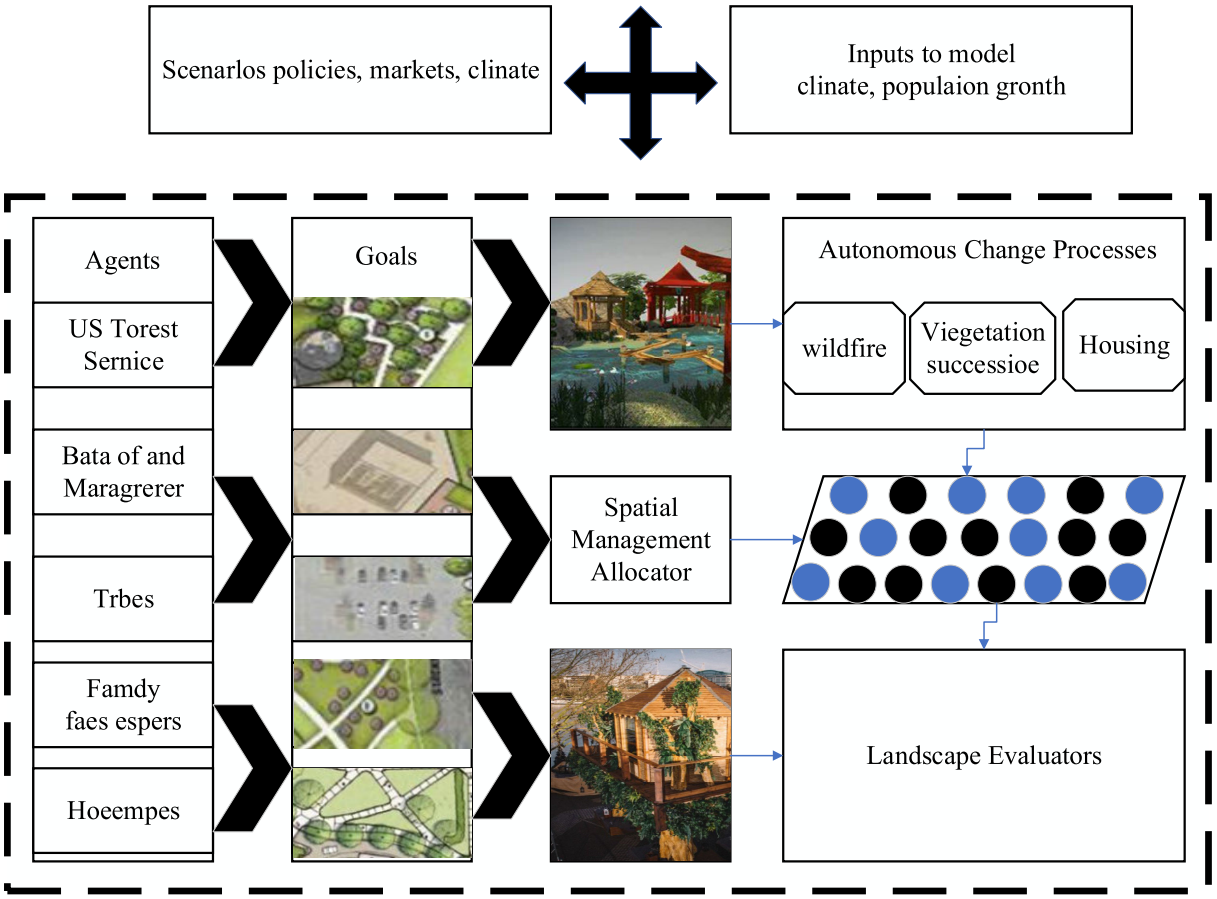

FIGURE 3. Garden graphics optimization model.

the requirements of the WDBN learning algorithm. In the experiment, to ensure the learning effect and efficiency of WDBN, the number of neurons in the input layer, output layer, and the hidden layer should be designed reasonably. Although too many neurons can improve the functioning of the network, it will prolong the learning of the neural network. Time increases the operating burden of the computer and waste computer resources. For the design of the number of neurons, there is no universal analytical formula that can be applied. In realistic applications, the design is combined with the characteristics of different projects. This article selects the appropriate number of neurons according to the requirements of handwritten text recognition, as shown in Figure 3.

Since the birth of wavelet transforms, with the continuous expansion and innovation of wavelet transform by researchers, there are many different wavelet basis functions, such as Morlet, Harr, and other wavelet basis functions. The choice of wavelet basis function will directly affect the result and efficiency of the wavelet transform, so the choice of wavelet basis function must be determined by actual conditions. Considering that the research object of this paper is handwritten text images, according to the characteristics of handwritten text, and the most used and simplest Morlet wavelet in engineering applications as the wavelet base for transformation, this paper adopts Morlet wavelet function as the activation function of DBN. The error gradient descent method is used to continuously optimize the network so that the parameters are constantly updated, and finally, the actual output value of the network structure model is constantly close to the expected value, to reach the optimal network structure. the entire network training process, the weight of the network is the threshold is constantly updated [35]. In the process of network construction, the number of network layers is determined first, and then the number of neurons in each neural network layer, the activation function is selected and the learning rate is determined, and the network construction is completed.

The feasibility of the combination of the particle swarm algorithm and WDBN: First, as the particle swarm algorithm in the intelligent optimization algorithm, it has excellent global search capabilities. It can search for the weights and thresholds of WDBN, avoiding the indiscriminate assignment of random values. The combination of the two can improve the generalization ability and learning performance of WDBN and also improve its convergence speed; the second is that WDBN mainly relies on the update of weights and thresholds in the training process of the network model to achieve the optimization of the network model. The particle swarm algorithm happens to be able to achieve a global search by constantly updating the speed and position of particles

in discrete dimensions. The error between the actual output value and the expected value is considered as the fitness value. The smaller the fitness value, the stronger the particle's optimization ability [36]. The particles move continuously in the weight space in WDBN to minimize the error in the output layer of the network. The update speed of the particles in the network weight. As the speed of the particles is continuously updated, the output error is continuously reduced. This method makes the error iteration stops. when the entire algorithm is over, the weight set of the network model is the result, so far, the network model training is completed [37].

III. SIMULATION DESIGN OF GARDEN GRAPHICS VISUAL EFFECTS

A. RESEARCH ON GARDEN GRAPHIC DATA

Table 1 is the 15 data sets used in this experiment, which is selected from the UCI machine learning library. The number of features in these data sets ranges from 13 with the smallest wine to 310 with the largest LSVT. Therefore, very extreme requirements are put forward for the optimization ability of the algorithm.

TABLE 1. Data set information.

Databases	Feature number	Number of samples	Number of categories
Wine	25	20	36
Australian	38	29	35
Vehicle	21	24	40
Parkinsons	31	33	35
German	35	33	28
WBCD	33	40	28
Ionosphere	36	22	21
Spect f	37	26	25
Lung Cancer	21	37	35
Sonar	30	35	27
Iibras	27	30	29
Hillvalley	39	24	30
musk 1	38	26	29
Arrhythmia	21	22	37
LSVT	30	40	32

During the experiment, each data set was split into an 80% training set and a 20% test set. Each particle represents a subset of features. The selected feature subsets in the training set are used to measure the classification performance through ten-fold crossover and five-nearest neighbor (5∼NN) methods. At the end of the algorithm, the particle set in the external document obtained in the training set is measured using the test set.

The specific parameters of the algorithm are as follows, $a = 0.02$ proposed in the local search, the size of the population $N = 30$, the maximum number of iterations is 100, and the size of the external document is 30. The common parameter settings of the methods proposed in this paper are the same: the random value is in the interval [1.5, 2.0], and the inertia weight o takes the random value in the interval [0.1, 0.5], with the largest particle speed $Vmax = 0.6$, minimum speed $Vmin = -0.6$, and threshold $= 0.6$. In NSGA-II and BMOABC algorithms, binary coding is used. Each particle is composed of D binary strings, where D is the dimension of the particle. The value of each bit is 0 indicating that the feature is not enabled, and the value 1 indicates that the feature is select. The mutation probability in the NSGA-II algorithm is one, and the crossover probability is 0.9. In the BMOABC algorithm, the limit parameter $Dlimit = 100$ and the parameter $T = 1000$. For each data set, it runs independently 40 times.

For each data set, since it needs to run 40 times independently, the external documents obtained from each run are combined into a union. In this union, for feature subsets with the same number of features, calculate their average classification error rate. Also, all non-dominated solutions in the union are called the optimal solution, and the classification error rate of the optimal solution is calculated. Firstly, HMISO is compared with MOPSO and CMDPSO, which prove that HMISO improves the performance of the PSO algorithm by combining mutual information. And Figure 4 is the comparison of HMISO, NSGA-II, and BMOABC algorithms on the test set. In these figures, ''-A'' represents the average classification performance obtained by 40 independent runs, and ''-B'' represents the classification performance of the optimal solution obtained by 40 independent runs. The X-axis is equal to the number of features selected by the particle, the Y-axis represents the classification error rate, and the right above the graph represents the data set name and feature dimensions and the classification error rate without feature selection.

Aiming at the problem of garden graphics detection, we promoted this program on the Windows7 platform. Use Matlab R2016a is a software development tool. This article uses the GA_PSO algorithm to optimize the W-kNN algorithm and takes 7 optimal fitness values iterated by the GA_PSO algorithm as the weight vectors of the 7 sample features. This step can enhance the accuracy of feature classification, and then use W-kNN classifier to classify these features. In this experiment, using the GA_PSO algorithm to optimize the W-kNN algorithm can improve the accuracy of classification to a large extent, to better solve and avoid the problem that the algorithm is easy to fall into the restricted optimal solution.

B. EVALUATION OF INDEX ANALYSIS

Owing to the large amount of sample data in the CASIA-HWDB1.0 database, more computer resources will be consumed during actual calculations, which will overload the computer. To avoid the above situation, 90% of the sample set is selected as the experimental data, and 90% of the experimental data is separated into a training set and a validation set. There are three common methods: leave out method, cross-validation method, and self-service method. To guarantee the stability and fidelity of the evaluation results, this paper adopts the cross-validation method. First, the sample set D is

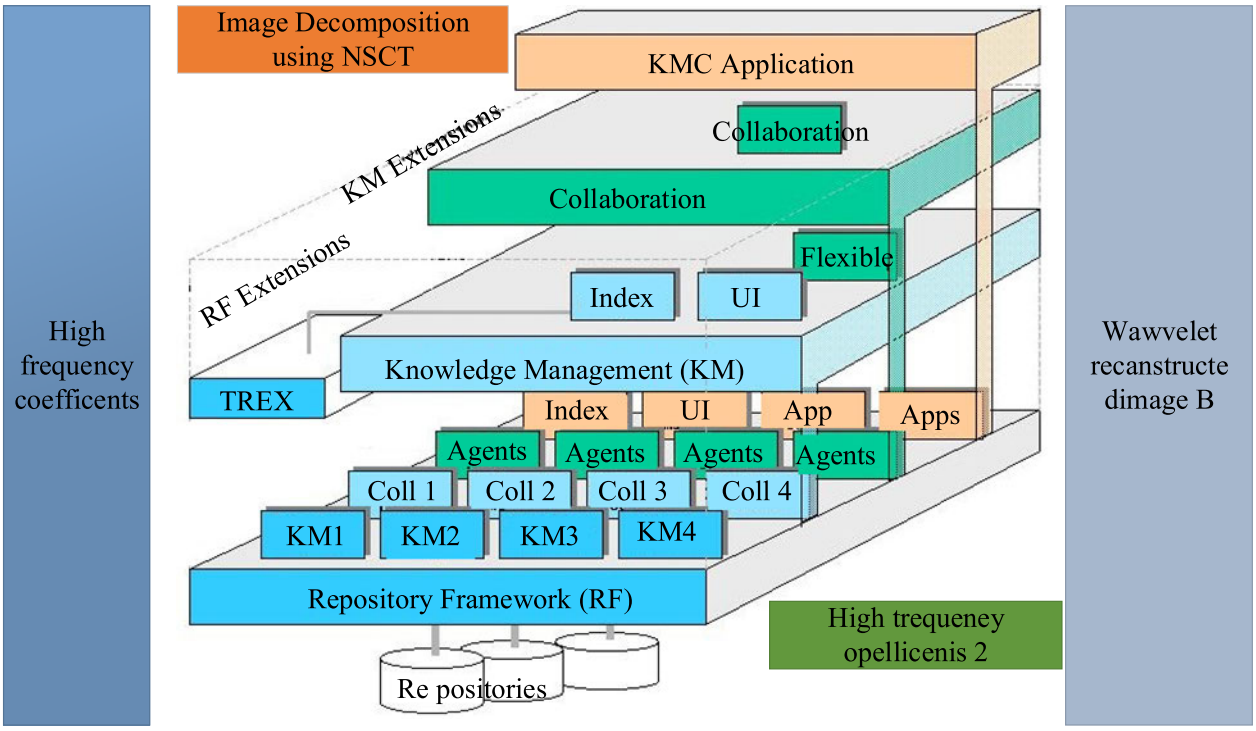

FIGURE 4. Schematic diagram of visual effect simulation of garden graphics.

divided into K groups of data sets of the same size, and then 2K groups of sample sets are used as the training data set for training, and the remaining part as the verification set, and so on, until all the sample sets are traversed, and finally the K sets of verification error rates are averaged, and the average verification error rate is regarded as the generalization error rate. The larger the value of K, the more data set it divides, the higher the reliability of the final generalization error rate, but the corresponding time is larger. In practical applications, K is usually taken, as shown in Figure 5.

Because deep learning fully convolutional neural network is very complex, it will take a lot of time to train, and the network level of the fully convolutional network is very deep, so the result of the model is possible while conducting specific experiments. It will stay near the optimal solution, which may affect the experimental results: on the other hand, it will make the convergence time of the entire model longer.

When performing semantic segmentation operations on separate garden pictures, because it is impossible to completely segment each object correctly, sometimes the garden scenery element category in a certain garden image is regarded as another garden scenery element category. This will lead to some inaccuracy in the results obtained in this article, and the fully convolutional neural network model used in this article can accomplish the goal of semantic segmentation of the pixel level of the garden scene in the complex garden image. This paper studies the final segmentation result and the real image for comparison and compares with the real garden image, according to the category classification results

FIGURE 5. Schematic diagram of the cross-validation method.

obtained in this paper, the original garden image is digitized, and the final output digital result is regarded as the final result of the classification of garden elements in the final garden image. Using this as the criterion, the model was analyzed for segmentation accuracy and compared. This article will count the pixel errors in the garden image to determine the result of the classification of landscape elements. This article uses the more popular semantic segmentation criteria to perform accurate statistics.

This section outlines some theories of the classification of landscape elements, fully convolutional neural networks, and image segmentation, and introduces related technological research. First, the landscape elements are classified into

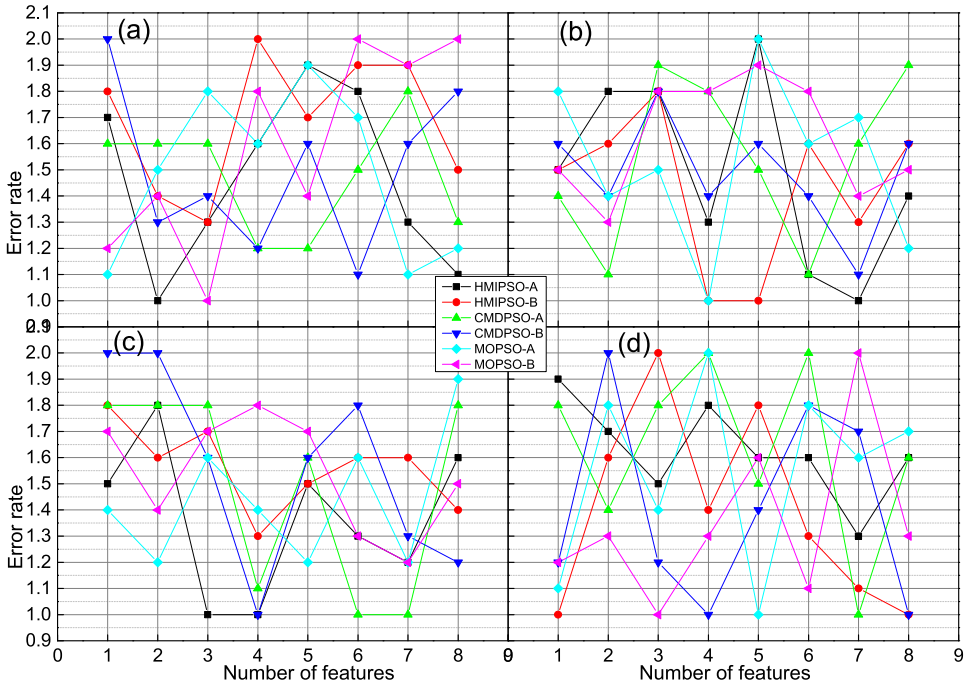

FIGURE 6. Experimental results on the test set.

heaven, ground, water, and ecological four major categories of scenery. Then it provides an overview of the fully convolutional neural network and specifically describes the structure and function of the fully convolutional neural network. Finally, the current segmentation algorithm of garden images is summarized, which provide the basis for the semantic segmentation later. This section also introduces the fully convolutional neural network mentioned in the paper, using the theoretical basis of the previously mentioned convolutional network, on this basis, leads to the fully convolutional neural network further explain how to use FCN network to complete the end-to-end semantic segmentation of the image, as well as the principle and processing process.

IV. RESULTS ANALYSIS

A. THE IMPACT OF IMPROVING ALGORITHMS ON THE CLASSIFICATION

The information directly above Figure 6 is the classification error rate and the number of corresponding features evaluated by using all available features for discrete data sets. The feature dimension of data set musk is 166, and the classification error rate obtained by using these 166 features to classify is 16.843%. The Pareto frontier (indicated by "-B" in the figure) obtained by using the HMISO algorithm proposed in this paper for feature selection, the maximum classification error rate is 28.617%, the number of features is 12; the minimum classification error rate is 13.124%, and the number is 27. It can be seen that although the classification error rate corresponding to the minimum number of features obtained using the HMISO algorithm is greater than the error rate of classification without feature selection, the error rate corresponding to the maximum number of features obtained in the optimal solution is higher than that without feature selection. The classification error rate was reduced by 3.783%, and the number of features was also decreased by 139.

The wine feature dimension of the data set is 13, and the classification error rate obtained by using these 13 features to classify is 30.883%. In the optimal solution obtained by using the HMISO algorithm proposed in this paper for feature selection, the maximum classification error rate is 9.73%, which is a reduction of 21.543%, the number of features is 1, which reduces the number of 12 features; the minimum classification error rate is 1.57%, Which is reduced by 29.243%, the number of features is 4, and the number of features is reduced by 9. The use of HMIPSO for classification of the data set wine not only reduces the number of features but also decreases the classification error rate. According to the above analysis, the classification using the HMIPSO algorithm can effectively reduce the classification error rate and greatly reduce the number of features compared to directly utilizing all the features for classification.

It can be observed in Figure 7 that most of the optimal solution set obtained by the HMIPSO multi-objective feature selection method proposed in this paper is better than the MOPSO and CMDPSO methods. And as the dimension of the feature increases, the HMISO effect becomes more observable. For example, it can be seen from Figure 7 that on some data sets with smaller dimensions, the advantage of the HMISO effect is not very noticeable. For example, for the German dataset with a dimension of 24, the classification error rate obtained by the MOPSO algorithm is 21.647%, and the number of features is 1. The maximum feature classification error rate obtained by the CMDPSO algorithm is 23.050%, the number of features is

2, and the minimum classification The error rate is 22.677%, and the number of features is 5; when the German feature number is 2 and the feature number is 4 obtained by the HMISO algorithm, the corresponding error rates are 25.647% and 21.040%, respectively. According to the experimental results of the German data set, although the maximum number of features of the HMISO algorithm is larger than the number of features obtained by the MOPSO algorithm, the classification error rate is reduced by 0.677%; compared with the CMDPSO algorithm, although the minimum classification error rate is greater than that of CMDPSO algorithm. The number of features is less than the CMDPSO algorithm. At the same time, when the number of features in the CMDPSO algorithm is 5, the classification error rate is 22.677%, which is higher than the number of features in the HMISO algorithm, which is 4, and the classification error is 1.627%. Therefore, even though the Pareto frontier obtained by HMIPSO algorithm is not completely better than the other two algorithms, it also improves the quality of understanding to a certain extent.

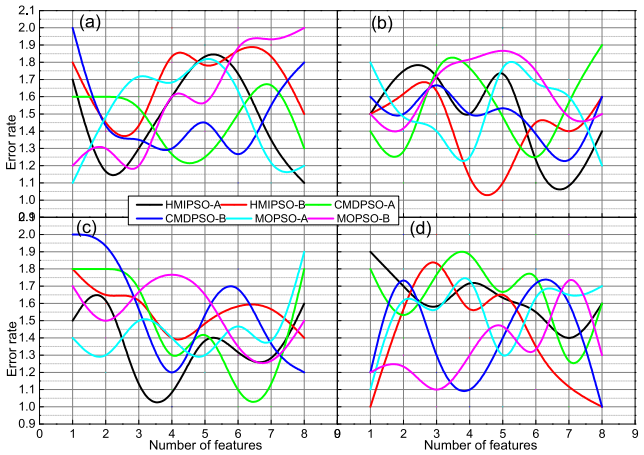

FIGURE 7. Experimental results on the test set.

Use an adaptive perturbation strategy to perturb the population to avoid the problem that the PSO algorithm converges too fast when performing a global search and causes the particles to become premature and fall into the local optimum; and for specific feature selection problems, the mutual information method can express the dependence of the data itself. For the advantage of the degree, the Pareto front surface generated by each iteration of the population is locally learned, and a multi-objective feature selection method (HMIPSO) that mixes mutual information and particle swarm algorithm is proposed. HMIPSO can effectively make particles add relevant features or delete irrelevant and redundant features, play a valuable role in exploring the particles, improve the performance of the population, and enrich the diversity of the particles in the search. By comparing on 15 data sets, it can not only improve the performance of the PSO algorithm on the multi-objective feature selection problem but also outperform the two fresh comparison algorithms proposed.

Studies have shown that ultrasonic waves interfered by noise appear as non-stationary signals, and often appear as narrow sudden changes. After the Gaussian noise signal is superimposed with ultrasonic, the following characteristics will be shown in Figure 8. Figure 8(a) is the forehead burr noise generated by noise interference, Figure 8(b) is the supersonic noise signal caused by local noise, Figure 8(c) is the ultrasonic signal submerged by noise, Figure 8(d) is the details of the ultrasonic signal.

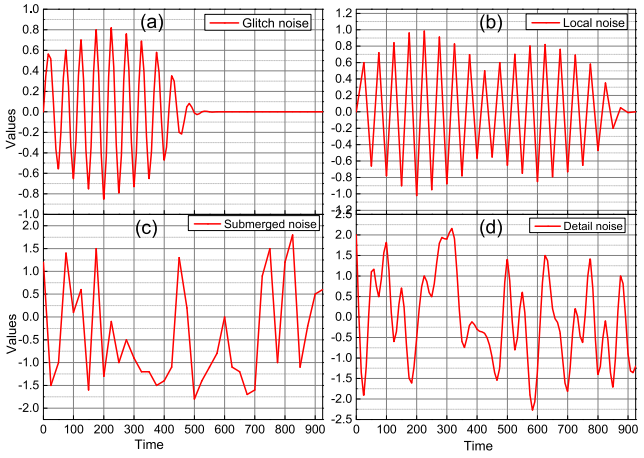

FIGURE 8. Graphic noise processing results.

B. SELECTION OF THE NUMBER OF LAYERS OF GARDEN IMAGES AND ANALYSIS OF EXPERIMENTAL RESULTS

In the wavelet threshold denoising method, the choice of the number of layers determines the integrity of the signal decomposition. If the number of decomposition layers is too low, it will cause the original signal and the noise signal to match the characteristics of the signal is not obvious, if the number of decomposition layers is too large, the signal error is relatively large.

Therefore, for the selection of the number of stratifications, this paper first selects the approximate range of the number of stratifications with the help of an empirical method and selects 2-9 layers to increase the rigor of the experiment. For the selection of other parameters, after the analysis of the previous section, the selected wavelet base is used to determine Sym7 and Sym5 in different situations in the previous section. Also, the selection of additional parameters is still the same as in the previous section. Figure 9 shows the evaluation index of blocks noise signal after using the wavelet soft threshold denoising method.

The analysis in Figure 9 shows that when the noise signal of blocks uses the wavelet soft threshold denoting method, the root means square error (RMSE) is the smallest and the signal-to-noise ratio (SNR) is the largest when the 4 layers are selected under the Sym7 wavelet base., the smoothness (P) is also relatively small, and the cross-correlation coefficient

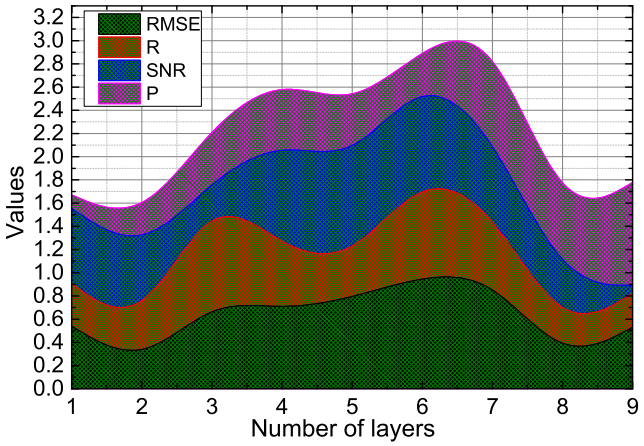

FIGURE 9. Soft threshold noise reduction evaluation index value of the garden image.

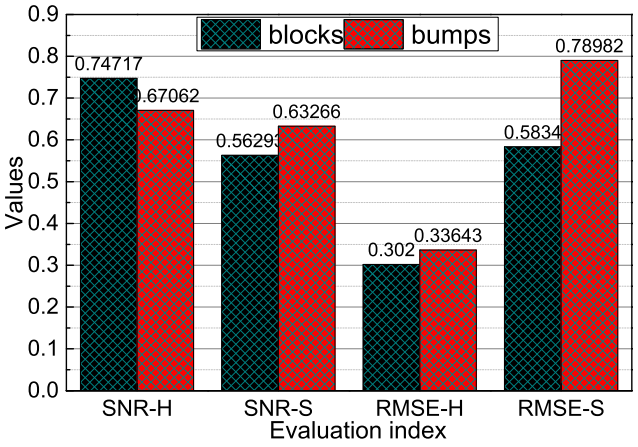

FIGURE 11. Denoising results of garden images.

(R) is relatively large, achieving the best noise reduction performance.

In this section, to verify the effect of improving the wavelet threshold denoting method, the blocks and bumps signals that come with matter are introduced. Because the denoising effects of blocks and bumps signals have public data, the denoising effects of different denoising methods can be performed. For intuitive comparison, first, use the two signals for experimentation. The two signals are presented in figure 10.

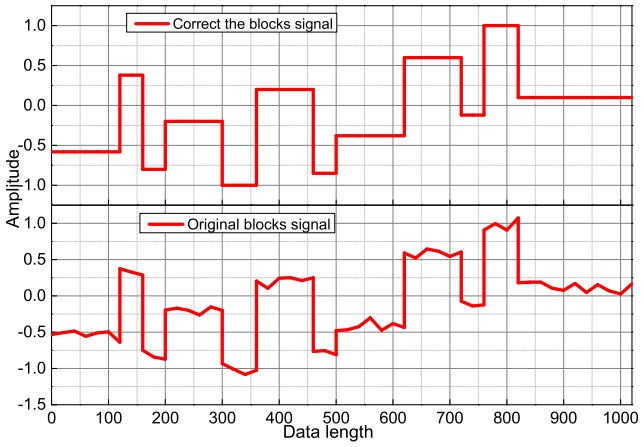

FIGURE 10. Pure signal and noise signal.

The analysis shows that as the number of wavelet decomposition layers continues to increase, different wavelet bases have roughly the constant changes in their composite evaluation values. The number of layers of wavelet transform is from 2 to 4, and the composite evaluation value gradually decreases. From 4 to 9 layers, the composite evaluation value slightly increases. The composite evaluation value has a minimum value in 4 layers. Depending on the meaning of the composite evaluation value, the optimal decomposition layer parameter of the wavelet is 4 layers. When the Sym7 wavelet base is selected for the blocks noise signal, the composite evaluation value is the smallest. Depending on the meaning of the composite evaluation value, the optimal wavelet basis parameter of the wavelet is the Sym7 wavelet basis; when the Sym6 wavelet basis is selected for the bumps noise signal, the composite evaluation value is the smallest. The meaning of composite evaluation value, the optimal wavelet basis parameter of wavelet is a Sym6 wavelet basis.

Based on the traditional Donohoe global threshold, a logarithmic function is put in place to construct a wavelet adaptive threshold. The improved adaptive threshold can slowly decrease with the stepwise increase of the wavelet decomposition scale. Because as the wavelet decomposition scale increases, the concentration of noise will also be diluted, and the amplitude of the noise figure will reduce as the wavelet decomposition scale increases. The adaptive threshold replaces the constant invariance of the global threshold and can adapt to the change in the amplitude of the noise figure as the wavelet decomposition scale increases. The improved wavelet adaptive threshold can realize the use of different thresholds on different wavelet decomposition scales, which effectively avoids excessive stifling of effective signals in the threshold quantization process, and retains as much effective information as possible so that the image is not affected by noise reduction distortion.

It can be seen from the above analysis process that the wavelet soft and hard threshold denoting method is used for the noise signals of blocks and bumps. By analyzing the changing trend and minimum point of the composite evaluation value, the wavelet basis function, and the number of layers in the wavelet threshold denoising parameter can be obtained. The selection is unified into one method. Therefore, for the noise signal of blocks, using Sym7 and Sym5 wavelet basis functions and 4 layers of layers can achieve the best noise reduction effect; for noise signals of bumps, using the Sym5 wavelet basis function and 4 layers of layers can achieve the best noise reduction effect.

Figure 11 shows the denoising results obtained by the method in this paper. The comparison between the two shows that the debasing effect of the wavelet denoting parameter selection method based on the composite evaluation value is

FIGURE 12. Simulation results of garden graphics optimization.

better than the denoting results in the literature, which proves that the wavelet base and the number of layers are selected uniformly in this paper. The idea can be carried out, and the denoising effect diagram is shown in Figure 11.

The choice of the wavelet basis and the number of layers in the wavelet threshold denoting method is experimentally analyzed, and a method for uniformly determining the wavelet threshold denoting parameters based on the composite evaluation value is proposed. This method is utilized to experiment on the noise signals of blocks and bumps. The verification proves the feasibility of the method; finally, the method applies to the noise reduction of ultrasonic noise signals.

C. ANALYSIS OF SIMULATION RESULTS

Observe the comparison of the effects of the six noise reduction algorithms in Figure 12. The noise reduction effect of traditional wavelet hard and soft threshold functions is not ideal. Four words ''national restaurant'' in the image are not clear enough and difficult to recognize, and there are still many noise points in the sky. Because the wavelet hard threshold function is used to decrease noise, it can be observed that there are some faintly visible block-like structures in the image after the noise reduction process. It is precisely because of the discontinuity of the wavelet hard threshold function that the wavelet is reconstructed this Pseudo-Gibbs phenomenon occurs only when oscillations occur. Some pixels in the image after the noise reduction process have become blurred. It is precisely because the wavelet soft threshold function has quantitatively shrunk the estimated wavelet coefficients and is lost some valid information. It can be observed that the image contrast is subtle, there are still a few noise points, and the detail texture is not smooth enough, and there are a few more abrupt pixels. Figure 12 only uses the improved wavelet adaptive threshold function to reduce noise. This shows that in the process of image noise reduction, some high-frequency information is filtered out, the edge of the image target is not fully protected, and the sharpness of the image is also gloomy.

Figure 12 is a bilateral filtering algorithm using the improved combined noise reduction algorithm of this article, combined with an improved wavelet adaptive threshold function and an improved gray-scale filter kernel function. From the subjective evaluation point of view, the image quality is very close to the original reference image in Figure 12, the contrast is greatly enhanced, the edge of the image target is also fully protected, and the background in the image is very delicate.

Digital image processing includes an image preprocessing stage and a subsequent deep processing stage. Noise reduction belongs to the image preprocessing stage. It provides a solid guarantee for image segmentation, fusion, recognition, and other post-depth processing, and its role is crucial. This paper constructs an improved wavelet threshold function based on the customary threshold function. The function is continuous and uninterrupted in the entire domain, and there is no constant deviation between the estimated wavelet coefficients and the original wavelet coefficients, which better restrict the traditional threshold. This makes the Pseudo-Gibbs phenomenon not appear after the image is reconstructed, and improves the accuracy of the image after reconstruction. Also, a simulation experiment is performed on the adjustable parameter p in the function, and the analysis of the image mean square error, peak signal-to-noise ratio and structural similarity after noise reduction shows that the three data indicators all tend to be flat after the p-value is 4. While ensuring the effect of noise reduction, to reduce the computational complexity of the algorithm, the parameter p is set to a value of 4 in succeeding experiments.

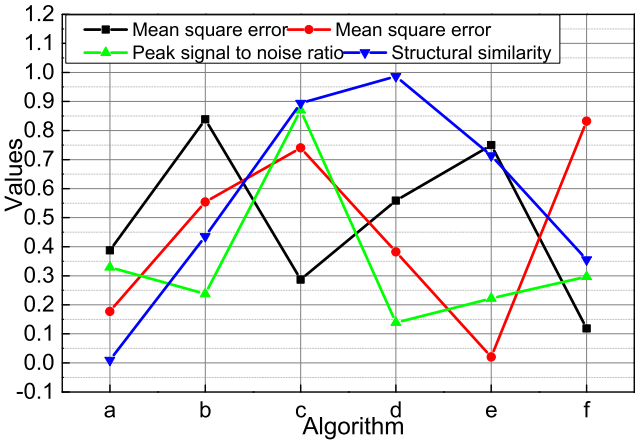

FIGURE 13. Comparison of image quality evaluation data.

It can be seen from Figure 13 that the three indexes of MSE, PSNR, and SSIM of the noise reduction results of the algorithm in this paper are better than the first five algorithms, and the noise reduction effect of the traditional wavelet hard and soft threshold functions has been greatly improved. The method has similar limitations with the wavelet soft threshold function, and it does not address the problem of losing effective information very well. Combining the wavelet soft threshold function and the traditional bilateral filter, the noise reduction effect is still not ideal when no improvement is

proposed for the two algorithms. After the algorithm in this paper introduces a bilateral filter with improved gray filter kernel function, the PSNR using only the improved wavelet adaptive threshold function method is increased by nearly 0.543, and the SSIM is also increased to nearly 0.853, that is, the similarity to the original image is close to 83.40 %. This data fully proves the feasibility of the algorithm in this paper, and the experimental simulation shows that the improved combined algorithm studied in this paper has achieved a relatively ideal noise reduction effect.

Firstly, it briefly summarizes the basic knowledge of spatial filtering and introduces two commonly used spatial filtering methods to pave the way for the ensuing discussion of bilateral filtering. Secondly, a detailed algorithm introduction to bilateral filtering is carried out, explaining its working principle, and analyzing its strengths. Then analyze and study the limitations of the bilateral filter, and found that there are numerous neighboring pixels with a large gray difference from the center pixel in a filter window. These unrelated neighbor pixels will also participate in the filtering. Aiming at this limitation, the gray filter kernel function in the bilateral filter is improved to minimize the influence of extraneous pixels in the filter window on the central pixel. The improved bilateral filtering improves the performance of protecting the edges of image targets. Then introduce the image noise reduction operation steps of the improved combined algorithm researched in this article. Using this algorithm to reduce image noise requires four steps. Finally, the MATLAB platform is used to conduct a comparative experimental simulation of six noise reduction algorithms, and the algorithm in this paper is compared with several other traditional algorithms. The simulation results are shown in two ways, subjective evaluation, and objective evaluation. Experimental datum shows that the improved combined algorithm proposed in this paper has an ideal image noise reduction effect compared with traditional algorithms.

V. CONCLUSION

In the context of studying the classification of landscape elements in garden images, this paper conducts in-depth research on the technologies and methods involved and mentioned in the image semantic segmentation model. For the classification of landscape elements in garden images, deep learning technology is undoubtedly the best solution so far. Therefore, given many landscape elements in garden images and the large changes in the environment, this thesis takes the landscape elements in garden images as the research object, studies the semantic segmentation of garden images, and comprehensively applies the two-stage training of the model. Algorithms such as digital image processing and full convolutional neural network structure analyze the classification of garden elements in garden images, and finally realize the semantic segmentation of garden elements in garden images based on the fully convolutional neural network model, which is the future garden scene. The study of element classification provides a certain foundation. The gray filter kernel function in habitual bilateral filtering is improved, a filter threshold is constructed, and it is improved into a piecewise function. The advantage of this is that the neighboring pixels with a large gray difference from the center pixel are not involved in filtering at all, reducing the impact of irrelevant neighbor pixels on the center pixel in a filtering window, and improving the ability of bilateral filtering to protect the edge of the image target. Through simulation and comparison experiments, combining bilateral filtering with wavelet adaptive threshold function, the image visual effect, mean square error, peak signal-to-noise ratio, and structural similarity after noise reduction is better than traditional noise reduction algorithms.

REFERENCES

[1] V. Tripathi, A. Mittal, D. Gangodkar, and V. Kanth, "Real time security framework for detecting abnormal events at ATM installations," *J. Real-Time Image Process.*, vol. 16, no. 2, pp. 535–545, Apr. 2019.
[2] E. Aghajari and G. D. Chandrashekhar, "Self-organizing map based extended fuzzy C-means (SEEFC) algorithm for image segmentation," *Appl. Soft Comput.*, vol. 54, pp. 347–363, May 2017.
[3] B. Yang, L. Zhang, F. W. B. Li, X. Jiang, Z. Deng, M. Wang, and M. Xu, "Motion-aware compression and transmission of mesh animation sequences," *ACM Trans. Intell. Syst. Technol.*, vol. 10, no. 3, pp. 1–21, May 2019.
[4] S. D. Pendleton, W. Liu, H. Andersen, Y. H. Eng, E. Frazzoli, D. Rus, and M. H. Ang, "Numerical approach to reachability-guided sampling-based motion planning under differential constraints," *IEEE Robot. Autom. Lett.*, vol. 2, no. 3, pp. 1232–1239, Jul. 2017.
[5] G. Munda, C. Reinbacher, and T. Pock, "Real-time intensity-image reconstruction for event cameras using manifold regularisation," *Int. J. Comput. Vis.*, vol. 126, no. 12, pp. 1381–1393, Dec. 2018.
[6] P. D. Cristóforis, M. A. Nitsche, T. Krajník, and M. Mejail, "Real-time monocular image-based path detection," *J. Real-Time Image Process.*, vol. 11, no. 2, pp. 335–348, Feb. 2016.
[7] Y. Zhou, H. Hu, Y. Liu, S.-W. Lin, and Z. Ding, "A real-time and fully distributed approach to motion planning for multirobot systems," *IEEE Trans. Syst., Man, Cybern. Syst.*, vol. 49, no. 12, pp. 2636–2650, Dec. 2019.
[8] Y. Jiang, J. Wang, Y. Liang, and J. Xia, "Combining static and dynamic features for real-time moving pedestrian detection," *Multimedia Tools Appl.*, vol. 78, no. 3, pp. 3781–3795, Feb. 2019.
[9] F.-C. Ghesu, B. Georgescu, Y. Zheng, S. Grbic, A. Maier, J. Hornegger, and D. Comaniciu, "Multi-scale deep reinforcement learning for real-time 3D-landmark detection in CT scans," *IEEE Trans. Pattern Anal. Mach. Intell.*, vol. 41, no. 1, pp. 176–189, Jan. 2019.
[10] Z. Hou, Y. Dong, J. Xiang, X. Li, and B. Yang, "A real-time QRS detection method based on phase portraits and box-scoring calculation," *IEEE Sensors J.*, vol. 18, no. 9, pp. 3694–6702, Mar. 2018.
[11] T. Long, T. Zeng, C. Hu, X. Dong, L. Chen, Q. Liu, Y. Xie, Z. Ding, Y. Li, Y. Wang, and Y. Wang, "High resolution radar real-time signal and information processing," *China Commun.*, vol. 16, no. 2, pp. 105–133, Mar. 2019.
[12] A. J. Alzahrani and J. Khan, "Robust approach of edge detection in videos using spatial-temporal features," *Int. J. Comput. Sci. Issues*, vol. 15, no. 6, pp. 42–48, Nov. 2018.
[13] B. Dong, C. N. Morrison, C. C. Branas, T. S. Richmond, and D. J. Wiebe, "As violence unfolds: A space–time study of situational triggers of violent victimization among urban youth," *J. Quant. Criminol.*, vol. 36, no. 1, pp. 119–152, Mar. 2020.
[14] J. Shao, B. Du, C. Wu, and L. Zhang, "Can we track targets from space? A hybrid kernel correlation filter tracker for satellite video," *IEEE Trans. Geosci. Remote Sens.*, vol. 57, no. 11, pp. 8719–8731, Nov. 2019.
[15] J. F. P. van Amerom, D. F. A. Lloyd, M. Deprez, A. N. Price, S. J. Malik, K. Pushparajah, M. P. M. van Poppel, M. A. Rutherford, R. Razavi, and J. V. Hajnal, "Fetal whole-heart 4D imaging using motion-corrected multi-planar real-time MRI," *Magn. Reson. Med.*, vol. 82, no. 3, pp. 1055–1072, Sep. 2019.
[16] P. Kandhway and A. K. Bhandari, "Spatial context cross entropy function based multilevel image segmentation using multi-verse optimizer," *Multimedia Tools Appl.*, vol. 78, no. 16, pp. 22613–22641, Aug. 2019.

[17] T. F. H. Runia, C. G. M. Snoek, and A. W. M. Smeulders, "Repetition estimation," *Int. J. Comput. Vis.*, vol. 127, no. 9, pp. 1361–1383, Sep. 2019.
[18] X. X. Wang, X. M. Zhao, and Y. Shen, "A video traffic flow detection system based on machine vision," *J. Inf. Process. Syst.*, vol. 15, no. 5, pp. 1218–1230, Oct. 2019.
[19] G. Maulucci, F. Di Giacinto, C. De Angelis, O. Cohen, B. Daniel, C. Ferreri, M. De Spirito, and S. Sasson, "Real time quantitative analysis of lipid storage and lipolysis pathways by confocal spectral imaging of intracellular micropolarity," *Biochimica et Biophysica Acta (BBA)-Mol. Cell Biol. Lipids*, vol. 1863, no. 7, pp. 783–793, Jul. 2018.
[20] A. Majumdar and R. Tedrake, "Funnel libraries for real-time robust feedback motion planning," *Int. J. Robot. Res.*, vol. 36, no. 8, pp. 947–982, Jul. 2017.
[21] Y. Zhang, J. Wang, X. Wang, and J. M. Dolan, "Road-segmentation-based curb detection method for self-driving via a 3D-LiDAR sensor," *IEEE Trans. Intell. Transp. Syst.*, vol. 19, no. 12, pp. 3981–3991, Dec. 2018.
[22] E. S. Ebbini, C. Simon, and D. Liu, "Real-time ultrasound thermography and thermometry [life sciences]," *IEEE Signal Process. Mag.*, vol. 35, no. 2, pp. 166–174, Mar. 2018.
[23] L. Shahmiri, S. Tavassoli, and S. N. H. Jouybari, "Detecting and counting vehicles using adaptive background subtraction and morphological operators in real time systems," *J. Adv. Comput. Eng. Technol.*, vol. 5, no. 4, pp. 213–220, Nov. 2019.
[24] Y. J. Heo, D. Lee, J. Kang, K. Lee, and W. K. Chung, "Real-time image processing for microscopy-based label-free imaging flow cytometry in a microfluidic chip," *Sci. Rep.*, vol. 7, no. 1, pp. 1–9, Sep. 2017.
[25] Y. Wang, B. Jin, Y. Wang, D. Wang, X. Liu, and Q. Bai, "Real-time distributed vibration monitoring system using Φ-OTDR," *IEEE Sensors J.*, vol. 17, no. 5, pp. 1333–1341, Mar. 2017.
[26] B. Reily, F. Han, L. E. Parker, and H. Zhang, "Skeleton-based bio-inspired human activity prediction for real-time human–robot interaction," *Auton. Robots*, vol. 42, no. 6, pp. 1281–1298, Aug. 2018.
[27] K. S. Chandrasekar and P. Geetha, "Highly efficient neoteric histogram–entropy-based rapid and automatic thresholding method for moving vehicles and pedestrians detection," *IET Image Process.*, vol. 14, no. 2, pp. 354–365, Feb. 2020.
[28] J. Yin, N. Wang, and A. N. Perakis, "A real-time sequential ship roll prediction scheme based on adaptive sliding data window," *IEEE Trans. Syst., Man, Cybern. Syst.*, vol. 48, no. 12, pp. 2115–2125, Dec. 2018.
[29] P.-H.-C. Chen, K. Gadepalli, R. MacDonald, Y. Liu, S. Kadowaki, K. Nagpal, T. Kohlberger, J. Dean, G. S. Corrado, J. D. Hipp, C. H. Mermel, and M. C. Stumpe, "An augmented reality microscope with real-time artificial intelligence integration for cancer diagnosis," *Nature Med.*, vol. 25, no. 9, pp. 1453–1457, Sep. 2019.
[30] S. Dreha-Kulaczewski, A. A. Joseph, K.-D. Merboldt, H.-C. Ludwig, J. Gärtner, and J. Frahm, "Identification of the upward movement of human CSF *in vivo* and its relation to the brain venous system," *J. Neurosci.*, vol. 37, no. 9, pp. 2395–2402, Mar. 2017.
[31] C. Zheng, K. W. Bieri, Y.-T. Hsiao, and L. L. Colgin, "Spatial sequence coding differs during slow and fast gamma rhythms in the hippocampus," *Neuron*, vol. 89, no. 2, pp. 398–408, Jan. 2016.
[32] F. S. Marzano, E. Picciotti, S. Di Fabio, M. Montopoli, L. Mereu, W. Degruyter, C. Bonadonna, and M. Ripepe, "Near-real-time detection of tephra eruption onset and mass flow rate using microwave weather radar and infrasonic arrays," *IEEE Trans. Geosci. Remote Sens.*, vol. 54, no. 11, pp. 6292–6306, Aug. 2016.
[33] H. Mattern, A. Sciarra, F. Lüsebrink, J. Acosta-Cabronero, and O. Speck, "Prospective motion correction improves high-resolution quantitative susceptibility mapping at 7T," *Magn. Reson. Med.*, vol. 81, no. 3, pp. 1605–1619, Mar. 2019.
[34] S. Aminikhanghahi, T. Wang, and D. J. Cook, "Real-time change point detection with application to smart home time series data," *IEEE Trans. Knowl. Data Eng.*, vol. 31, no. 5, pp. 1010–1023, May 2019.
[35] M. Capogrosso, F. B. Wagner, J. Gandar, E. M. Moraud, N. Wenger, T. Milekovic, P. Shkorbatova, N. Pavlova, P. Musienko, E. Bezard, J. Bloch, and G. Courtine, "Configuration of electrical spinal cord stimulation through real-time processing of gait kinematics," *Nature Protocols*, vol. 13, no. 9, pp. 2031–2061, Sep. 2018.
[36] K. Zhao, J. Deng, and D. Cheng, "Real-time moving pedestrian detection using contour features," *Multimedia Tools Appl.*, vol. 77, no. 23, pp. 30891–30910, Dec. 2018.
[37] R. Weitschat and H. Aschemann, "Safe and efficient human–robot collaboration part II: Optimal generalized human-in-the-loop real-time motion generation," *IEEE Robot. Autom. Lett.*, vol. 3, no. 4, pp. 3781–3788, Oct. 2018.

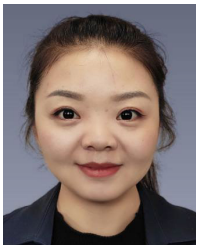

HUA ZHANG graduated from Jiangxi Science and Technology Normal University, in 2011, and received the M.F.A. degree from the Academy of Fine Arts and Design, Northwest Normal University, in 2013. Since 2013, she has been a Teacher with the School of Fine Arts, Weinan Normal University, where she is currently a Lecturer in fine arts. She has taught the courses, including sketch, chromatics basis, oil painting, and history of Chinese and foreign arts. She has published more than 15 academic articles, hosted or participated in a variety of provincial or municipal scientific projects, and received several awards.

XIONGFEI MIN graduated from the Baoji University of Arts and Sciences, in 2005, and received the Sports master's degree from Xi'an Physical Education University, in 2010. Since 2010, he has been with Weinan Normal University, where he is currently a Lecturer in physical education. He has served as the Student Administrator and a Teaching Administrator at the School Physical Education. He has also taught tennis courses. He has published about ten academic articles and hosted or participated in scientific research projects at provincial and municipal levels.